

High Performance Airfoil Using Co-Flow Jet Flow Control

Ge-Cheng Zha*

Dept. of Mechanical and Aerospace Engineering
University of Miami
Coral Gables, Florida 33124
E-mail: zha@apollo.eng.miami.edu

Bruce F. Carroll †

Dept. of Mechanical and Aerospace Engineering
University of Florida
Gainesville, FL 32611-6250

Craig D. Paxton‡ and Clark A. Conley§

Dept. of Mechanical and Aerospace Engineering
University of Miami
Coral Gables, Florida 33124

Adam Wells ¶

Dept. of Mechanical and Aerospace Engineering
University of Florida
Gainesville, FL 32611-6250

Abstract

The wind tunnel tests in this research have proved the superior performance of co-flow jet(CFJ) airfoil to dramatically increase lift, stall margin, and drag reduction. Two airfoils with different injection slot size are tested to study the effect of geometry. The airfoil with smaller injection slot size (0.65% chord length) performs significantly better than the one with twice larger slot size. With the momentum coefficient varying from 0.1 to 0.30, compared with the baseline airfoil, the maximum lift of the smaller size CFJ airfoil is increased by 113% to 220%,

* Associate Professor, AIAA Member

† Associate Professor

‡ Graduate Student

§ Senior Undergraduate Student

¶ Graduate Student

the angle of attack (AoA) operating range (stall margin) is increased by 100% to 153%. The minimum drag coefficient is reduced by 30% to 127% with the momentum coefficient varying from 0.055 to 0.192. Large negative drag (thrust) is produced when the momentum coefficient is high. A coefficient of jet kinetic energy is introduced, which appears to correlate better with the maximum lift and stall margin than the momentum coefficient when CFJ airfoil geometry varies. The momentum coefficient correlates well with drag reduction. It is observed that the thicker injection slot airfoil has smaller stall AoA and hence less maximum lift. To achieve the same lift coefficient of 4.42, the power required for the thicker injection slot is 3.9 times of that required for the thinner injection slot airfoil. No optimization of the airfoil configuration is done in this research and hence it is believed that there is a great potential for further CFJ airfoil performance improvement.

In the experiment, it is observed that there is a limit of the jet mass flow rate to maintain the stability of the flow. Below the limit, increasing the jet mass flow rate (momentum coefficient) will make the flow attached and increase the lift and stall AoA. However, if the jet mass flow rate exceeds the limit, the whole flow field breaks down. This research also has conducted a concept study by CFD simulation indicating that it is possible for the CFJ airfoil to exceed the inviscid limit of maximum lift coefficient due to the high jet velocity inducing high suction velocity of the airfoil.

1 Introduction

To achieve high performance aircraft design, revolutionary technology advancement should be pursued to dramatically reduce the weight of aircraft and fuel consumption, significantly increase aircraft mission payload and maneuverability. Both the military and commercial aircraft will benefit from the same technology.

Flow control (FC) is the most promising route to break through the conventional aerodynamic design limit and bring dramatic performance improvement to aircraft[1, 2, 3]. NASA, Air Force and aerospace industry have recently made great efforts to develop flow control technology[4, 5, 6, 7]. To enhance lift and suppress separation, various flow control techniques have been used, including rotating cylinder at leading and trailing edge[8][9][3], circulation control using tangential blowing at leading edge and trailing edge[10][11][12] [13][14][15][16], multi-element airfoils[17][18], pulsed jet separation control[19][20][21][22], etc.

When a flow control technique is developed, there may be three issues needed to be considered: 1) Effectiveness: the FC method should have substantial improvement of aerodynamic performance, which primarily includes lift enhancement, drag reduction, and stall margin increase (suppression of separation) ; 2)Energy efficient: the FC method should not cause significantly more energy expenditure. Otherwise, the penalty may outweigh the benefit for the whole aircraft as a system. This includes minimal penalty to the propulsion system, minimal weight increase due to the FC system; 3) Easy implementation: the FC technique should not be too difficult to be implemented.

The rotating cylinder method is generally most effective when the leading edge or trailing edge are thick, and hence may be more applicable to low speed airfoil. It also needs a system to drive the rotating system and can increase aircraft weight. The multi-element airfoil can generate high lift, but generally comes with large drag and weight penalty due to the moving parts. In addition, the high lift flap system increases noise during landing.

A circulation control(CC) airfoil [16, 15] relies on local favorable pressure gradient on a curved surface to make the flow attached, the Coanda effect. Such favorable pressure gradient exists at the airfoil leading edge due to the suction and at the end of the trailing edge due to the low base

pressure when the trailing edge is blunt. To make the CC airfoil effective, the blunt TE is hence needed. However, this will create large drag at cruise. To overcome the dependence on large TE for circulation control airfoil, a movable flap at the airfoil TE is suggested by Englar [10]. The moving parts will increase the weight penalty to the aircraft. At large AoA, because the mainflow can not resist the large adverse pressure gradient, the local TE favorable pressure gradient can not be achieved and hence the Coanda effect is difficult to maintain. If only TE blowing is used, the CC airfoil will usually stall at a smaller AoA than the regular non-controlled airfoil[23]. To increase stall margin, the LE blowing needs to be added[23].

The other considerably high penalty of CC airfoil to the propulsion system is the dumped blowing jet mass flow. The blowing air for the wing is usually from the engine compressor bleed. The mass flow rate of the engine bleed is directly proportional to the decrease of thrust, i.e. an engine will suffer 1% thrust decrease for 1% bleed flow used for wing flow control, and suffer 1-3% fuel consumption increase depending on whether the bleed is from the compressor front stage or back stage.

To avoid the jet mass flow rate penalty due to blowing, the synthetic jet or pulsed jet with open or close loop feed back control are used[19, 20]. These methods need the jet generation system, complicated actuation and sensor systems, which may increase the degree of difficulty to implement the FC system and increase the weight of the aircraft as well. Since the interaction of the synthetic jet with the main flow is generally weak, the effectiveness to enhance lift and suppress separation may not as dramatic as desired. For example, the results shown in [19] using the periodic synthetic jet have about 35% increase of the C_{Lmax} and little increase of stall AoA, while the CFJ airfoil tested in this research increase the C_{Lmax} and AoA range by 220% and 153% respectively with $C_{\mu} = 0.28$. A movable flap is also used with the synthetic jet flow control airfoil studied in [19], which will increase the aircraft weight.

The new airfoil flow control technique using co-flow jet (CFJ) recently suggested by Zha and Paxton[24] is aimed at considering all the three issues mentioned above: effectiveness, energy efficient, and easy implementation. The co-flow jet airfoil is to open an injection slot near leading edge and a suction slot near trailing edge on the airfoil suction surface. The slots are opened by translating a great portion of the suction surface downward. A high energy jet is then injected near leading edge tangentially and the same amount of mass flow is sucked in near trailing edge. The turbulent shear layer between the main flow and the jet causes strong turbulence diffusion and mixing, which enhances lateral transport of energy from the jet to mainflow and allows the main flow to overcome severe adverse pressure gradient and remain attached at high angle of attack(AoA). The co-flow jet airfoil can dramatically enhance lift, reduce drag and increase stall margin based on CFD simulations[24]. The CFJ airfoil can recirculate the jet mass flow and hence can significantly reduce the penalty to propulsion system due to avoiding dumping the jet mass flow.

The objective of this research is to prove the superior performance of coflow jet airfoil concept by wind tunnel tests. At a certain AoA, a CFJ airfoil always achieves a significantly higher lift due to the augmented circulation. The operating range of AoA, hence the stall margin, is significantly increased. The energized main flow will fill the wake deficit and dramatically reduce the airfoil drag, or even generate thrust (negative drag). The filled wake will also reduce noise due to weakened wake mixing. In addition, a CFJ airfoil wing does not need a high lift flap system, which will further reduce noise during landing. A coflow jet airfoil does not rely on the Coanda effect at leading or trailing edge and the thick leading or trailing edge are not required. Hence the low form drag of modern airfoils can be maintained. The CFJ technique can be applied to any type of airfoil, including low speed thick airfoils and high speed thin airfoils.

Since a CFJ airfoil blows and sucks the same amount of mass flow, the jet mass flow then can be recirculated through the propulsion system instead of being dumped away. This can significantly reduce the penalty of energy expenditure to the overall airframe-propulsion system when compared to the blowing only method. The co-flow jet can be always on during the whole fly mission. The lift enhancement and drag reduction can be controlled by adjusting the injection total pressure, hence the jet mass flow rate, during the mission according to different needs. No moving parts are required.

The coflow jet airfoil concept studied in this research appears to have the following advantages:

- 1) Very effective to enhance lift and suppress separation;
- 2) Dramatically reduce drag and can achieve very high C_L/C_D (infinity when $C_D = 0$) at low AoA(cruise), and very high lift and drag at high AoA(take off and landing);
- 3) Significantly increase AoA operating range and stall margin;
- 4) Have small penalty to the propulsion system;
- 5) Can be applied to any airfoil, thick or thin;
- 6) Can be used for whole flying mission instead of only take off and landing;
- 7) Can be used for low and high speed aircraft;
- 8) Easy implementation with no moving parts;

The above advantages of the CFJ airfoil may derive the following superior aircraft performances:

- 1) Extremely short distance for take off and landing;
- 2) Supersonic aircraft to have small wing size matching cruise need, but also have high subsonic performance (e.g. high lift low drag at $M < 1$);
- 3) High maneuverability, high safety and fast acceleration military aircraft;
- 4) Very economic fuel consumption;
- 5) Small wing span for easy storage, light weight and reduced skin friction and form drag;
- 6) Low noise due to no high lift flap system and weakened wake mixing.

The wind tunnel tests conducted in this research have proved the high performance of the CFJ airfoil. This is the beginning to study and understand the working principle of CFJ airfoil. It is hoped that this research will open a door to a new area of flow control technology for next generation advanced aircraft.

2 CFJ Airfoil Geometry

Fig.1 shows the baseline airfoil, NACA0025, and two airfoils with co-flow jet slots. The NACA0025 airfoil was selected as the baseline airfoil due to its large thickness to facilitate implementation of co-flow jet, internal ducts, and instrumentation. The chord length of the airfoil is 0.1527m and the span is 0.3m. The co-flow jet airfoils are named using the following convention: CFJ4dig-INJ-SUC, where 4dig is the same as NACA 4 digit convention, INJ is replaced by the percentage of the injection slot size to the chord length and SUC is replaced by the percentage of the suction slot size to the chord length. For example, the CFJ0025-065-196 airfoil has the injection slot height of 0.65% of the chord and the suction slot height of 1.96% of the chord. The new suction surface shape is a downward translation of the portion of the original suction surface between the injection and suction slot. The CFJ0025-131-196 is constructed in the same way by recessing the suction surface by 1.31% of the chord at the injection slot and 1.96% of the chord at the suction slot. The previous studies [25, 24] indicate that the suction slot size needs to be larger than the inlet slot size in order to suck in the same amount of jet mass flow without being choked. The injection and suction slot are located at 7.11% and 83.18% of the chord from the leading edge. The slot faces are normal to the suction surface to make the jet tangential to main flow.

The internal ducts for both the injection and suction slots are also illustrated in Fig.1, labeled as the high pressure and low pressure cavities. The high pressure flow is injected into the high pressure cavity and then passes through a block of Duocel aluminum foam. The Duocel foam acts as a baffle

that gives a uniform flow distribution downstream of the foam and generates a highly uniform co-flow jet, which is imperative to achieve 2D flow for the CFJ airfoil testing. CFD was used as a design tool to simulate the CFJ airfoils and their secondary flow ducts inside the wind tunnel. Very good 2-dimensionality is achieved based CFD analysis and is verified in the experiment. Both the injection and suction ducts are designed to have a continually converging or diverging shape to ensure that the throat is located at the injection and suction slots. CFD results are used to verify that the injection and suction slots can pass the required mass flow rate of 0.1kg/s under the experimental conditions.

Stress analysis of the CFJ airfoil designs show that the low pressure in the suction duct can cause a deflection of the airfoil suction surface. Thus two support pins are placed near the cantilevered end to avoid the deflection as shown in Fig.1.

3 Wind Tunnel Measurement Setup

3.1 Wind Tunnel

The AEROLAB educational wind tunnel shown in Fig.2 with the test section of $12'' \times 12'' \times 24''$ located at the University of Florida is used for this research. A TSI PIV system is used to capture flow visualization and velocity vector fields on the mid span location. The lift, drag, and pitching moment are measured by the strain gauges located on the sidewall sting tube.

The co-flow jet is injected through the sting tube into the high pressure cavity and is sucked through a suction manifold on the opposite side of the airfoil, illustrated in Figs.3 and 4. The injection system consists of a compressor and two large storage tanks that provides a continuous constant injection flow, which is controlled by choking the flow using a butterfly valve turned on and off by a Fisher control valve.

The airfoil is fixed on the sidewall sting on the injection side and is cantilevered on the suction side. To avoid the airfoil cantilevered end deflection touching wind tunnel wall and causing force translation, sufficient clearance is made on the cantilevered end wind tunnel wall as shown in Fig.4. To prevent air leaking from the wind tunnel, a sealed plexiglass box is mounted outside of the suction side wind tunnel wall as shown in Fig.2. The light weight and soft latex suction tubes minimize the force translation and connect the suction system with the airfoil through the transparent plexiglass box, which allows the PIV camera to visualize and measure the flow velocity vector fields. The latex tubes are internally reinforced by brass inserts to prevent tube collapse.

The external suction system consists of four 240 gallon vacuum tanks (shown in the background of Fig.2), one 60 gallon tank, one 80 gallon tank, and two vacuum pumps. This system provides suction for 12-30 seconds within the required mass flow rate range. The suction mass flow rate is controlled by choking the flow with a butterfly valve at the desired mass flow rate and is turned on and off by a ball valve.

3.2 Measurement Calibration

To take into account of the airfoil deflection effect, the lift and drag components are calibrated using a known weight at the center span of the airfoil in its testing configuration with the latex tubes attached. This calibration showed a highly linear trend for both lift and drag with the coefficient

of determination R^2 values of 0.9994 and 0.9995[26], respectively. Using Student's t-distribution, the uncertainty of lift and drag is given by:

$$\Delta = \frac{t\sigma}{\sqrt{n}} \quad (1)$$

where Δ is the uncertainty, t is the Student's t value for corresponding confidence level[26], σ is the standard deviation, n is the number of samples. For a 95% confidence level and $n=50$ samples, $t = 2.0105$.

The standard deviation ranges from 1 N(Newton) at lower AoA to 5 N at higher AoA for both lift and drag. This corresponds to standard deviation in terms of C_L and C_D of 0.031-0.153.

So the uncertainty in C_L and C_D would then be 0.008814 at lower AoA and 0.043 at higher AoA. Strain gauge measurements are taken at approximately 2/3 Hz. These single measurements are actually an average of 5 integrations of a digital signal with a two power line cycle integration time. The sampling rate is 300Hz. Two power line cycles is equal to 33.3ms. This comes to 10 samples for each integration.

To calculate the wind tunnel velocity, a differential pressure transducer is used to measure the dynamic pressure. The transducer measures the difference between the static pressure upstream of the test section and the stagnation pressure in the room. Pressure readings are taken at 1Hz. A correction factor is multiplied by the stagnation pressure to account for losses that occur in the tunnel inlet. Mass flow rates are measured using fixed orifice plates placed inside of the injection and suction supply ducts. Mass flow rates are calculated based on eq.(2):

$$q_m = \frac{CE\epsilon\pi d^2 \sqrt{2\rho_1 \Delta p}}{4} \quad (2)$$

where, q_m is the mass flow rate, C is the discharge coefficient, $E = 1/\sqrt{1-\beta^4}$, ϵ is the gas expansion factor, d the orifice diameter, D the pipe internal diameter, $\beta = d/D$, ρ_1 the upstream density, Δp is the differential pressure. All values are constant except density and differential pressure. The density is found by measuring the upstream temperature and pressure. Temperature readings are taken at 1Hz.

To calculate the total uncertainty of the mass flow rate, we need to take the square root of the sum of the squares as in the following equation for the mass flow rate.

$$\frac{\delta q_m}{q_m} = \left(\left(\frac{\delta C}{C} \right)^2 + \left(\frac{\delta \epsilon}{\epsilon} \right)^2 + \left(\frac{2\beta^4}{1-\beta^4} \right)^2 \left(\frac{\delta D}{D} \right)^2 + \left(\frac{2}{1-\beta^4} \right)^2 \left(\frac{\delta d}{d} \right)^2 + \frac{1}{4} \left(\frac{\delta \Delta p}{\Delta p} \right)^2 + \frac{1}{4} \left(\frac{\delta \rho_1}{\rho_1} \right)^2 \right)^{1/2} \quad (3)$$

Above data gives an uncertainty for injection mass flow rate, $\frac{\delta q_m}{q_m} = 0.164\%$ and for suction mass flow rate, $\frac{\delta q_m}{q_m} = 0.179\%$.

A Kiel probe was placed in the injection duct just downstream of the Duocel foam. This total pressure was then used to find the velocity of the injection jet. To determine the injection velocity, first the critical area ratio of a 1D duct A/A^* [27] is obtained by eq.(4):

$$\frac{A}{A^*} = \frac{KP_0 A_{jet}}{q_m \sqrt{T_0}} \quad (4)$$

Coefficient	Injection Mass Uncertainty	Suction Mass Uncertainty
$\frac{\delta C}{C}$	0.06	0.06
$\frac{\delta \epsilon}{\epsilon}$	0.144	0.144
$(\frac{2\beta^4}{1-\beta^4})^2 (\frac{\delta D}{D})^2$	≈ 0	≈ 0
$(\frac{2}{1-\beta^4})^2 (\frac{\delta d}{d})^2$	≈ 0	≈ 0
$\frac{\delta \Delta p}{\Delta p}$	0.100	0.176
$\frac{\delta \rho_1}{\rho_1} = \sqrt{\frac{\delta p_1}{p_1}^2 + \frac{\delta T_1}{T_1}^2}$	0.018	0.001

The $\frac{A}{A^*}$ can be also determined by[27]:

$$\frac{A}{A^*} = \frac{1}{M} \left[\left(\frac{2}{\gamma+1} \right) \left(1 + \frac{\gamma-1}{2} M^2 \right) \right]^{\frac{\gamma+1}{2(\gamma-1)}} \quad (5)$$

Where, $K=0.040416$, P_0 is the total pressure in injection slot, A_{jet} is the injection slot area, q_m is the mass flow rate, T_0 is the measured total temperature at the injection slot, γ is the specific heat ratio taken the value of 1.4. The injection jet Mach number is found by linearly interpolating the table of A/A^* and Mach number determined by eq.(5). The injection velocity is then calculated by the following relation:

$$V = M \sqrt{\gamma R T} \quad (6)$$

Static pressure is measured in the exit of the suction duct at the plane where the suction duct and suction manifold meet. This value is used to find the density, velocity, and total pressure in the suction duct.

The pitching moment measurement is not considered as reliable because the effect of the latex tubes is too difficult to calibrate for varying angle of attack. The pitching moment results hence are not presented in this paper and will be reported in the future research.

4 Results and Discussion

The chord length of the airfoil is 0.1527m and the freestream Mach number is about 0.11. This gives the Reynolds number about 3.8×10^5 , which is in the laminar/transitional region. To make the boundary layer fully turbulent in order to mimic the realistic flight conditions, the airfoil leading edge is tripped to trigger the turbulence.

4.1 CFJ Airfoil Performance

Fig.5 is the comparison of measured lift coefficient for the baseline NACA0025 airfoil and the CFJ0025-065-196 airfoil with the injection total pressure coefficient given(the last number in the legend, normalized by freestream total pressure). During a test, the injection total pressure is held as constant while the AoA varies. A higher injection total pressure will yield a higher injection momentum coefficient, and hence a higher lift coefficient and stall margin. The bottom two curves with circle and cross symbols are for the baseline NACA0025 airfoil with and without LE trip.

It shows that the one with trip delays stall by about 4 degree of AoA. This is because the fully turbulent boundary layer with the trip is more resistant to flow separation. The very bottom curve is the CFJ airfoil without the jet on. It has less stall AoA than the baseline airfoil because the injection and suction slot steps weaken the boundary layer and make separation occur at a smaller AoA.

Table 1 lists the aerodynamic parameters of the baseline NACA0025 airfoil and the CFJ0025-065-196 airfoil with injection total pressure coefficient of 1.27. Table 1 indicates that the C_{Lmax} of the CFJ0025-065-196 airfoil is 3.2 times of the baseline airfoil, which is a 220% increase. The AoA stall margin is defined as the interval of the zero lift AoA to stall (maximum lift) AoA. The AoA stall margin of CFJ0025-065-196 airfoil is hence 2.53 times of the baseline airfoil stall margin, an increase of 153%.

Airfoil	$AoA_{C_L=0}$	$C_{\mu_{C_L=0}}$	$AoA_{C_{Lmax}}$	C_{Lmax}	$C_{\mu_{C_{Lmax}}}$	$C_{Dmin}(AoA = 0^\circ)$
Baseline NACA0025	0°	0.0	19°	1.57	0.0	0.128
CFJ0025-065-196	-4°	0.187	44°	5.04	0.28	-0.036

Table 1: Comparison of aerodynamic parameters between baseline airfoil and CFJ airfoil.

For the CFJ0025-065-196 airfoil, at injection total pressure coefficient 1.19, wind tunnel tests are also done to see the effect of the LE trip. The tripped one (dash-dot line with square symbol) delays stall by 4 degree of AoA. This is because the trip on the airfoil enhances the turbulence mixing on the suction surface and is hence more resistant to stall.

Fig.6 and 7 are the flow visualization of the baseline NACA0025 airfoil at AoA of 10° and 20° , respectively. They show that the flow is attached at AoA of 10° and separated at AoA of 20° , which is consistent with the lift coefficient vs AoA given in Fig.5.

Fig.8 and 9 are the PIV measured normalized velocity (V/V_∞) contours and streamlines of the attached flow of the baseline NACA0025 airfoil at AoA of 10° , front part and rear part of the airfoil. They clearly show again that the flow is very well attached at AoA of 10° with the peak suction acceleration in the LE region. The flow merges to the mainflow in the TE region.

Fig.10 and 11 are the PIV measured normalized velocity (V/V_∞) contours and streamlines of the separated flow of the baseline NACA0025 airfoil at AoA of 20° , front part and rear part of the airfoil. They clearly show that the baseline airfoil flow is separated at AoA of 20° .

Fig.12 and 13 are the flow visualization of the CFJ0025-065-196 airfoil at AoA of 43° and 46° . They show that the flow is attached at AoA of 43° and massively separated at AoA of 46° , which is consistent with the lift coefficient vs AoA given in Fig.5.

Fig.14 and 15 are the PIV measured normalized velocity (V/V_∞) contours and streamlines of the attached flow of CFJ0025-065-196 airfoil at AoA of 43° , front part and rear part of the airfoil. The AoA of 43° is right before the stall AoA of 45° . They clearly show again that the flow is very well attached at AoA of 43° with very high peak suction acceleration in the LE region. The flow merges to the mainflow in the TE region. The momentum coefficient at AoA of 43° is $C_\mu = 0.3$.

Fig.16 and 17 are the PIV measured normalized velocity (V/V_∞) contours and streamlines of the separated flow of CFJ0025-065-196 airfoil at AoA of 46° , front part and rear part of the airfoil. They clearly show that the flow is massively separated at AoA of 46° .

Since the PIV was not able to measure the flow field below the airfoil for the current setup, a

CFD simulation for the 2D flow field of CFJ0025-065-196 airfoil at 39° AoA was conducted to have a qualitative understanding of the flow field. To make the flow attached, the momentum coefficient used in the computation is 0.33 and is significantly higher than the experiment value of 0.286. Fig.18 is the streamlines and Mach contours of the CFJ0025-065-196 airfoil flow field calculated at AoA of 39° at freestream Mach number of 0.103. What is different from the usual flow field is that the stagnation point is far below the LE and is located at about the 1/3 chord point.

Fig.19 is the injection momentum coefficient of the CFJ0025-065-196 airfoil at three different injection total pressure. The momentum coefficient is defined as:

$$C_\mu = \frac{\dot{m}_j V_j}{0.5 \rho_\infty U_\infty^2 S} \quad (7)$$

Where \dot{m}_j is the co-flow jet mass flow rate, V_j the injection jet velocity, ρ_∞ and U_∞ the freestream density and velocity, S the wing area (chord \times wing span).

The injection mass flow rate and velocity are determined by the injection total pressure and the mainflow static pressure at the injection location. The injection total pressure is held constant while the AoA varies. When the AoA is increased, the LE suction is stronger and hence the local static pressure at the injection location decreases. The injection velocity therefore will increase, so will the mass flow rate and the momentum coefficient as shown in Fig.19. For the highest injection total pressure coefficient of 1.27, the momentum coefficient varies from 0.184 to 0.3. The lowest injection total pressure coefficient of 1.04 has the momentum coefficient varying from 0.05 to 0.1, which increase the C_{Lmax} by 113% and AoA stall margin by 100%. These results indicate that even the small momentum coefficient is very effective to enhance the lift and stall margin.

Fig. 20 is the drag polar of the CFJ0025-065-196 airfoil. The drag coefficient of CFJ airfoil is significantly reduced and have a small region of negative drag (thrust). For example, at $C_L=1$, for $C_\mu = 0.071$, the CFJ0025-065-196 airfoil drag reduction is 19%; for $C_\mu = 0.197$, the drag reduction is 90%, this makes the L/D increased by 10 times. At lower C_L value with the total pressure coefficient of 1.27, the drag reduction is over 100% because the drag is negative and becomes thrust. When the drag becomes zero or negative, the L/D may be not meaningful since it approaches infinity.

The drag reduction can be easily understood by doing a control volume analysis around the airfoil. The drag is determined by:

$$D = \int \int \rho U (U_\infty - U) dA \quad (8)$$

Where U is the wake velocity. When U is greater than U_∞ , the drag is negative and becomes thrust.

As pointed out in [24], at low AoA, the CFJ airfoil wake is filled with the energized mainflow and has inversed velocity deficit. In this case, the airfoil has no drag, but thrust. The airfoil drag can be decomposed to two parts: skin friction and pressure drag. The skin friction drag does not vary much when the AoA changes. It is the large pressure drag reduction that significantly decreases the total drag[24].

4.2 Slot Size Effect

To examine the effect of the slot size, the CFJ0025-131-196 airfoil is tested with the injection slot size twice as large as that of the CFJ0025-065-196 airfoil. The suction slot size is unchanged. The slot locations are also the same as those of CFJ0025-065-196 airfoil.

To study the effect only caused by the geometry, both the airfoils are tested with the same injection total pressure coefficient 1.04. Fig.21 is the comparison of injection jet velocity, which shows that the larger slot size airfoil has a slightly higher jet velocity at the same AoA before the airfoil stalls. The density of the CFJ0025-131-196 airfoil is slightly less than that of the CFJ0025-096-196. In general, the velocity and density are not very different for the two airfoils. This is because that the jet is mostly in the incompressible flow range. Fig. 23 shows that the injection jet mass flow rate of CFJ0025-131-196 airfoil is about twice as large as that of the CFJ0025-096-196 airfoil due to the larger slot area.

Fig. 24 is the lift comparison for the two airfoils. It shows that the lift coefficient of CFJ0025-131-196 is a little higher than that of CFJ0025-096-196 airfoil before the airfoil stall. The slightly higher lift is induced by the slightly higher jet velocity of CFJ0025-131-196. Obviously, the price paid with twice larger jet mass flow rate to gain this small benefit of lift is high. Further more, the CFJ0025-131-196 airfoil stalls at lower AoA than CFJ0025-096-196 airfoil even with about twice larger mass flow rate. The reason why the CFJ0025-131-196 airfoil with larger injection mass flow rate stalls earlier is not fully clear at this time. It is speculated that the large centrifugal force makes the jet detached from the curved airfoil suction surface.

Fig. 25 is the drag comparison for the two airfoils. The minimum drag of the CFJ0025-131-196 airfoil at AoA=0° is about 50% lower than that of the CFJ0025-131-196 airfoil. The reason is that the jet momentum coefficient of CFJ0025-131-196 airfoil is higher than that of the CFJ0025-096-196 airfoil due to the large jet mass flow rate and the mixing is enhanced. After mixing, the wake is filled more than the CFJ0025-096-196 airfoil.

Fig.26 is the comparison of the tested lift coefficient for baseline NACA0025 and CFJ0025-131-196 airfoil with different injection total pressure. Again, the C_{Lmax} and AoA stall margin are significantly increased. The stall AoAs are again less than those of the CFJ0025-096-196 airfoil and hence the magnitude of C_{Lmax} is also less. The jet mass flow rate is significantly higher than that of the CFJ0025-096-196 airfoil due to the twice larger injection slot size. This can be seen in Fig. 27 showing the measured injection momentum coefficient of CFJ0025-131-196 airfoil.

Fig.28 is the drag polar of the CFJ0025-131-196 airfoil with different injection total pressure. As shown in Fig.25, the minimum drag reduction of the CFJ0025-131-196 airfoil is significantly more than the CFJ0025-096-196 airfoil as shown in the drag polar of Fig. 20. There is a large negative drag (thrust) area.

Above results may indicate that, if the design purpose is to achieve high lift and stall margin, a small injection slot should be used; if it is to reduce drag, larger slot size should be used. There should be an optimum slot size to be the most energy efficient, which will be studied in next step.

The jet momentum coefficient is a good parameter to determine the performance of fixed geometry airfoils. Fig.29 is the ratio of the maximum lift of the two CFJ airfoils to the maximum lift of the baseline airfoil against the momentum coefficient C_μ . Fig. 30 is the ratio of the AoA stall margin of the two CFJ airfoils to that of the baseline airfoil against the momentum coefficient C_μ . The airfoil performance correlates well with the momentum coefficient for the fixed geometry. That is: when the geometry (slot size) does not change, increasing the momentum coefficient will

increase the stall margin and maximum lift coefficient. However, if all the results are combined together with different geometry (open and solid symbols), it is seen in Fig. 29 and Fig. 30 that, when the injection slot size varies, the test data are scattered and do not correlate well with the jet momentum coefficient.

To find a parameter to correlate airfoil performance independent of the geometry, it is found that the coefficient of jet kinetic energy per unit area seems a good one for C_{Lmax} and AoA stall margin. The coefficient of jet kinetic energy is defined as:

$$C_{jk} = \frac{\dot{m}_j V_j}{0.5 \rho_\infty U_\infty^2 S_{injection\ slot}} \quad (9)$$

Fig.31 is the ratio of the maximum CFJ lift of the two CFJ airfoils to the maximum lift of the baseline airfoil against C_{jk} . Fig. 32 is the ratio of the AoA stall margin of the two CFJ airfoils to that of the baseline airfoil against C_{jk} . Compared with Fig.29 and 30, Fig. 31 and 32 collapse much better. In general, when C_{jk} increases, the maximum lift and stall margin increase. Compare Fig.29 and Fig. 31, Fig.30 and Fig. 32, it can be seen that the thicker injection slot CFJ0025-131-196 airfoil (solid symbols) may have higher momentum coefficient than that of the thin injection slot airfoil, but in terms of the kinetic energy coefficient, they are less because the thicker slot airfoil stalls earlier and has lower jet velocity. Fig. 31 and 32 indicate that, when the kinetic energy coefficient varies from 14 to 50, the maximum lift of the CFJ airfoil is increased by 96% to 220%. The AoA stall margin is increased by 74% to 153%.

For drag reduction, the momentum coefficient correlates better with the test data than the jet kinetic energy coefficient, as shown in Fig. 33 and Fig. 34. The drag reduction is calculated with the minimum drag at AoA=0 by the following formulation:

$$Drag\ Reduction = (C_{Dcfj} - C_{Dbaseline})/C_{Dbaseline} \quad (10)$$

Table 1 indicates that the reduction of the minimum drag of CFJ0025-065-196 airfoil with jet momentum coefficient of 0.186 is 128.4%. Fig. 33 and Fig. 34 show that the reduction of the minimum drag of CFJ0025-131-196 airfoil with jet momentum coefficient of 0.50 is 300%. These results demonstrate that the CFJ airfoil is very effective to reduce drag. The drag reduction relies on filling the wake. The higher momentum coefficient generated by the thicker slot size airfoil is more effective. This says that the mechanism to enhance lift and stall margin is different from that to reduce drag. The former relies on higher jet kinetic energy to induce higher circulation and energize boundary layer. The latter relies on higher jet mass flow rate to fill the wake.

Since there are only 6 points collected in the tests of this research, the correlation based on C_{jk} mentioned above may not be conclusive and needs more measurement data to confirm in future research.

Fig. 35 and Fig. 36 show the injection and suction mass flow rate, which are set to be the same. They agree very well for most of the points except for one or two with the maximum difference within 3.9%.

Fig. 37 and 38 show the total pressure ratio at CFJ injection and suction for CFJ0025-065-196 and CFJ0025-131-196 airfoil. The total pressure ratio represents the power required to pump the CFJ. The total pressure ratio of the CFJ0025-065-196 airfoil is significantly lower than that of the CFJ0025-131-196 airfoil due to the smaller injection slot. The mass flow rate of CFJ0025-065-196 is hence far lower than that of CFJ0025-131-196. The overall power required for CFJ0025-065-196

to achieve the same lift coefficient will be much less than that of the CFJ0025-131-196 airfoil. For example, table 2 gives the comparison of the two airfoils to achieve the same lift coefficient 4.42. The jet mass flow rate of CFJ0025-065-196 is only half of that of CFJ0025-131-196. If assume the same efficiency for the secondary flow pumping system, the power to pump the CFJ0025-131-196 airfoil is then 3.9 times of that needed for CFJ0025-065-196 airfoil as shown in table 2.

Airfoil	C_L	\dot{m} (kg/s)	PR	AoA	Power Required (unit)
CFJ0025-065-196	4.42	0.051254	1.33	34.7°	1
CFJ0025-131-196	4.42	0.11	1.65	30°	3.9

Table 2: Comparison of power required to achieve $C_L = 4.42$ for the two CFJ airfoils.

This example indicates that there is a dramatic difference of power consumption (fuel consumption) by simply using different slot size to achieve the same lift. Totally only two slot sizes are tested in this study as concept proof. The airfoil configuration is not optimized. It is hence believed that there is a great room for further CFJ airfoil performance improvement if an optimum configuration study is done.

4.3 Jet Instability

In the experiment, it is observed that there is a limit of the jet mass flow rate to maintain the stability of the flow. Below the limit, increasing the jet mass flow (momentum coefficient) will make the flow attached and increase the lift and stall margin. However, if the jet mass flow rate exceeds the limit, the whole flow field breaks down and a large separation occurs as the jet does not exist. The turbulent shear layer due to jet mixing is complicated and is dominant by the coherent structure[28]. The reason of the flow field breakdown is not clear at this time and may be speculated as the following two aspects:

1) the mixing shear layer loses stability due to the large difference of the Mach number, or the so called convective Mach number,

$$M_c = \frac{U_1 - U_2}{a_1 + a_2} \quad (11)$$

where U_1, U_2, a_1 , and a_2 are the velocity and speed of sound of the main flow and the jet. The density and velocity ratio between the mainflow and jet also have an effect on the mixing shear layer stability[29][28].

2) The centrifugal force of the jet is too large that the jet becomes detached and the flow field collapses.

Due to the time limitation of this research, the details of the jet instability phenomenon was not studied. More detailed research of the jet stability limit from both CFD and experiment will be conducted in future.

5 Super-Circulation Airfoil

Conceptually, the CFJ airfoil should be able to break the inviscid C_{Lmax} limit when the CFJ induces higher flow velocity on the suction surface than the inviscid potential velocity. The inviscid maximum lift is given as[30]:

$$C_{Lmax} = 2\pi(1 + t/c) \quad (12)$$

where t/c is the ratio of the maximum thickness to chord.

The jet velocity of CFJ airfoil is controlled by the injection total pressure and the injection duct shape, and hence can be made greater than the inviscid velocity. The jet then may induce higher circulation on the airfoil than the inviscid flow. We term the airfoil with higher lift and hence higher circulation than that of the the inviscid limit as “Super-Circulation Airfoil”. The super-circulation airfoil is based on the hypothesis of steady state flow, that is the jet will remain attached no matter how high the jet velocity is. This may not be true as we have seen the jet instability problem in the wind tunnel tests. Nonetheless, there is enough evidence to believe that the Super-Circulation Airfoil is possible.

Based on the steady state assumption, we then use the RANS model CFD solver to simulate a highly cambered CFJ airfoil created from NACA0025. The airfoil is named CFJ11425-065-196. According to eq.(12), the inviscid limit of C_{Lmax} is 7.85. Fig. 39 is the streamlines and Mach contours of the CFJ11425-065-196 airfoil flow field at AoA of 39° with the jet momentum coefficient $C_\mu = 0.6$, $M_\infty = 0.1$. The lift coefficient calculated is $C_L = 9.74$, which is far greater than the inviscid limit. It is known that CFD over predicts the results. Nonetheless, the large amount exceeding the inviscid C_{Lmax} is encouraging. Fig. 39 also shows that the stagnation point is nearly located at mid-chord point, which is far below the leading edge where the stagnation point of a conventional airfoil locates.

Further study of the Super-Circulation Airfoil concept will be one of the future research tasks.

6 Conclusions

This research has successfully demonstrated the superior performance of co-flow jet airfoil concept in wind tunnel tests to dramatically increase lift, stall margin, and drag reduction. In the wind tunnel tests conducted in this research, two airfoils with different injection slot size are tested to study the effect of geometry. The airfoil with smaller injection slot size (0.65% chord length) performs significantly better than the one with twice larger slot size. With the momentum coefficient varying from 0.1 to 0.30, compared with the baseline airfoil, the maximum lift of the smaller size CFJ airfoil is increased by 113% to 220%, the angle of attack operating range (stall margin) is increased by 100% and 153%. The minimum drag coefficient is reduced by 30% to 127% with the momentum coefficient varying from 0.055 to 0.192. Large negative drag (thrust) is produced when the momentum coefficient is high. The L/D increase of CFJ airfoil is difficult to measure because when the drag is zero, $L/D = \infty$.

Under the same injection total pressure, the jet mass flow rate of the twice larger injection slot airfoil is about twice as large as that of the smaller slot airfoil. At the same AoA before stall, the gain using the larger injection slot in lift enhancement is small. The gain in minimum drag reduction

is more significant than the lift enhancement. The higher jet mass flow rate also yields smaller stall AoA. The reason is not fully clear at this time and is speculated due to the centrifugal force detaching the jet. To achieve the same lift coefficient of 4.42, the power required (fuel consumption) for the twice larger slot size airfoil is 3.9 times of that of the CFJ airfoil with smaller size. The two airfoils tested in this research are not optimized. It is hence believed that there is a great potential to further improve the CFJ airfoil performance when an optimum configuration study is done.

Based on the limited wind tunnel measurement data obtained in this research, a coefficient of jet kinetic energy is introduced, which appears to correlate better with the maximum lift and stall margin than the momentum coefficient when CFJ airfoil slot size varies. The minimum drag reduction correlates better with momentum coefficient. These correlation needs to be confirmed by more experimental data in future.

In the experiment, it is observed that there is a limit of the jet mass flow rate to maintain the stability of the flow. Below the limit, increasing the jet mass flow (momentum coefficient) will make the flow attached and increase the lift and stall AOA. However, if the jet mass flow rate exceeds the limit, the whole flow field breaks down and a large separation occurs as the jet does not exist. It is speculated that the instability may be attributed to the large dissimilarity of the jet and the main flow, and large centrifugal force of the jet when the jet velocity is high. The exact mechanism is not clear yet and will be studied in future research.

A concept study conducted by using CFD simulation in this research indicates that it is possible for the CFJ airfoil to exceed the inviscid limit of maximum lift coefficient due to the high jet velocity inducing high suction velocity of the airfoil. For a cambered CFJ airfoil modified from NACA0025, a lift coefficient of 9.7 is obtained by the CFD simulation, which is far greater than the inviscid maximum lift coefficient limit of 7.8. The concept is named Super-Circulation Airfoil.

The coflow jet airfoil concept studied in this research appears to have the following advantages: 1) Very effective to enhance lift and suppress separation; 2) Dramatically reduce drag and can achieve very high C_L/C_D (infinity when $C_D = 0$) at low AoA(cruise), and very high lift and drag at high AoA(take off and landing); 3) Significantly increase AoA operating range and stall margin; 4) Have small penalty to the propulsion system; 5) Can be applied to any airfoil, thick or thin; 6) Can be used for whole flying mission instead of only take off and landing; 7) Can be used for low and high speed aircraft; 8) Easy implementation with no moving parts;

The above advantages of the CFJ airfoil may derive the following superior aircraft performances: 1) Extremely short distance for take off and landing; 2) Supersonic aircraft to have small wing size matching cruise need, but also have high subsonic performance (e.g. high lift low drag at $M < 1$); 3) High maneuverability, high safety and fast acceleration military aircraft; 4) Very economic fuel consumption; 5) Small wing span for easy storage, light weight and reduced skin friction and form drag; 6) Low noise due to no high lift flap system and weakened wake mixing.

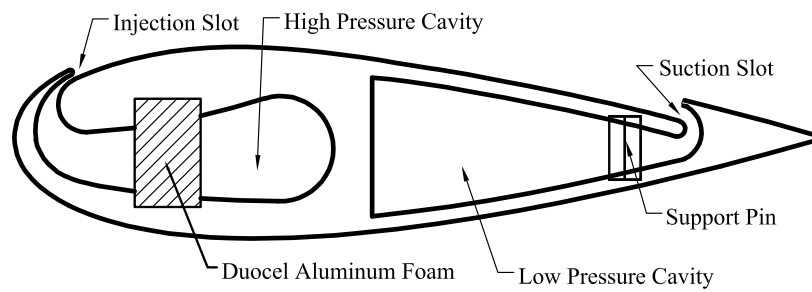
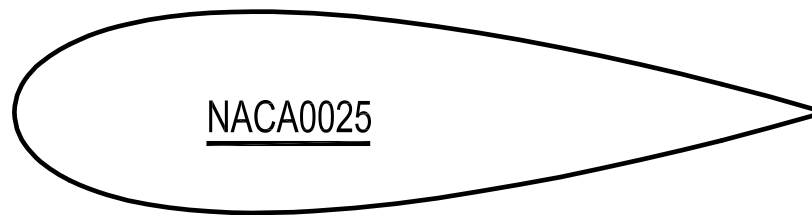
7 Acknowledgment

We would like to sincerely thank NASA LaRC for supporting this research as Phase I research of NRA-03-LaRC-02 under the contract NNL04AA39C. We would also like to thank Dr. R. Gaeta at Georgia Tech Research Institute for his advice to use Duocel aluminum foam to achieve uniform injection flow, which is crucial for the success of this research. We would like to thank Mr. Geoffrey A. Hill at NASA LaRC for discussion of possible application of CFJ airfoil to supersonic aircraft.

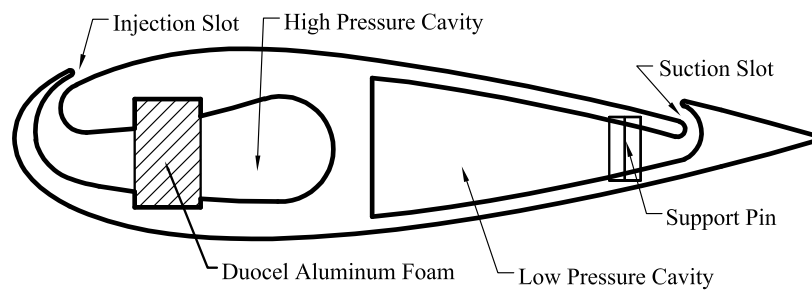
References

- [1] W. L. I. Sellers, B. A. Singer, and L. D. Leavitt, "Aerodynamics for Revolutionary Air Vehicles." AIAA 2004-3785, June 2003.
- [2] M. Gad-el Hak, "Flow Control: The Future ," *Journal of Aircraft*, vol. 38, pp. 402–418, 2001.
- [3] M. Gad-el Hak, *Flow Control, Passive, Active, and Reactive Flow Management*. Cambridge University Press, 2000.
- [4] S. Anders, W. L. Sellers, and A. Washburn, "Active Flow Control Activities at NASA Langley." AIAA 2004-2623, June 2004.
- [5] C. P. Tilmann, R. L. Kimmel, G. Addington, and J. H. Myatt, "Flow Control Research and Application at the AFRL's Air Vehicles Directorate." AIAA 2004-2622, June 2004.
- [6] D. Miller, , and G. Addington, "Aerodynamic Flowfield Control Technologies for Highly Integrated Airframe Propulsion Flowpaths." AIAA 2004-2625, June 2004.
- [7] V. Kibens and W. W. Bower, "An Overview of Active Flow Control Applications at The Boeing Company." AIAA 2004-2624, June 2004.
- [8] V. Modi, M. Fernando, and T. Yokomizo, "Drag Reduction of Bluff Bodies Through Moving Surface Boundary Layer Control." AIAA Paper No. 90-0298, 1990.
- [9] D. Cichy, J. Harris, and J. MacKay, "Flight Tests of a Rotating Cylinder Flap on a North American Rockwell YOY-10A Aircraft." NASA CR-2135, 1972.
- [10] R. J. Englar, "Circulation Control Pneumatic Aerodynamics: Blown Force and Moment Augmentation and Modifications; Past, Present and Future." AIAA 2000-2541, June 2000.
- [11] L. C. Bradley, "An Experimental Investigation of A Sting-Mounted Finite Circulation Control Wing." M.S. Thesis, Air Force Institute of Technology, 1995.
- [12] N. Wood, L. Robert, and Z. Celik, "Control of Asymmetric Vortical Flows over Delta Wings at High Angle of Attack," *Journal of Aircraft*, vol. 27, pp. 429–435, 1990.
- [13] N. Wood and L. Robert, "Control of Vortical Lift on Delta Wings by Tangential Leading-Edge Blowing," *Journal of Aircraft*, vol. 25, pp. 236–243, 1988.
- [14] N. Wood and J. Nielsen, "Circulation Control Airfoils-Past, Present, Future." AIAA Paper 85-0204, 1985.
- [15] R. J. Englar, L. A. Trobaugh, and R. Hemmersly, "STOL Potential of the Circulation Control Wing for High-Performance Aircraft," *Journal of Aircraft*, vol. 14, pp. 175–181, 1978.
- [16] R. J. Englar, "Circulation Control for High Lift and Drag Generation on STOL Aircraft," *Journal of Aircraft*, vol. 12, pp. 457–463, 1975.
- [17] A. Smith, "High-Lift Aerodynamics," *Journal of Aircraft*, vol. 12, pp. 501–530, 1975.
- [18] J. Lin, S. Robinson, R. McGhee, and W. Valarezo, "Separation Control on High Reynolds Number Multi-Element Airfoils." AIAA Paper 92-2636, 1992.

- [19] I. Wygnanski, “The Variables Affecting The Control Separation by Periodic Excitation.” AIAA 2004-2625, June 2004.
- [20] K. McManus and J. Magill, “Airfoil Performance Enhancement Using Pulsed Jet Separation Control.” AIAA Paper 97-1971, 1997.
- [21] K. McManus and J. Magill, “Separation Control in Incompressible and Compressible Flows Using Pulsed Jets.” AIAA Paper 96-1948, 1996.
- [22] H. Johari and K. McManus, “Visulation of Pulsed Vortex Generator Jets for Active Control of Boundary Layer Separation.” AIAA Paper 97-2021, 1997.
- [23] Y. Liu, L. N. Sankar, R. J. Englar, K. K. Ahuja, and R. Gaeta, “Computational Evaluation of the Steady and Pulsed Jet Effects on the Performance of a Circulation Control Wing Section.” AIAA Paper 2004-0056, 42nd AIAA Aerospace Sciences Meeting and Exhibit, Reno, Nevada 5 - 8 Jan 2004.
- [24] G.-C. Zha and C. Paxton, “A Novel Airfoil Circulation Augment Flow Control Method Using Co-Flow Jet.” NASA/ONR 2004 Circulation Control Workshop, 16-17 March 2004. AIAA Paper 2004-2208, June 2004.
- [25] G.-C. Zha, (team members: David Car, and W. Copenhaver), “Super Diffusion Cascades Using Co-Flow Jet Flow Control.” National Research Council Summer Faculty Final Report, Aug. 23, 2002.
- [26] J. P. Holman, *Experimental Methods for Engineers*. New York: McGraw-Hill, 7th Ed., 2001.
- [27] M. J. Zucrow and J. D. Hoffman, *Gas Dynamics*. John Wiley & Sons, New York, 1976.
- [28] G. Brown and A. Roshko, “On Density Effects and Large Scale Structure in Turbulent Mixing Layers,” *Journal of Fluid Mechanics*, vol. 64, pp. 675–816, 1974.
- [29] P. Strykowski, A. Krothapalli, and S. Jendoubi, “The Effect of Counterflow on the Development of Compressible Shear Layers,” *Journal of Fluid Mechanics*, vol. 308, pp. 63–69, 1996.
- [30] R. Englar and R. M. Williams, “Test Techniques for High Lift, Two Dimensional Airfoils with Boundary Layer and Circulation Control for Application to Rotary Wing Aircraft,” *Canadian Aeronautics and Space Journal*, vol. 19, pp. 93–108, 1973.



CFJ0025-065-196



CFJ0025-131-196

Figure 1: Airfoil section of the baseline airfoil of NACA0025, CFJ airfoil CFJ0025-065-196 and CFJ airfoil CFJ0025-131-196.



Figure 2: Wind tunnel setup and suction tanks.



Figure 4: CFJ airfoil showing the suction side.



Figure 3: CFJ airfoil showing the injection side.

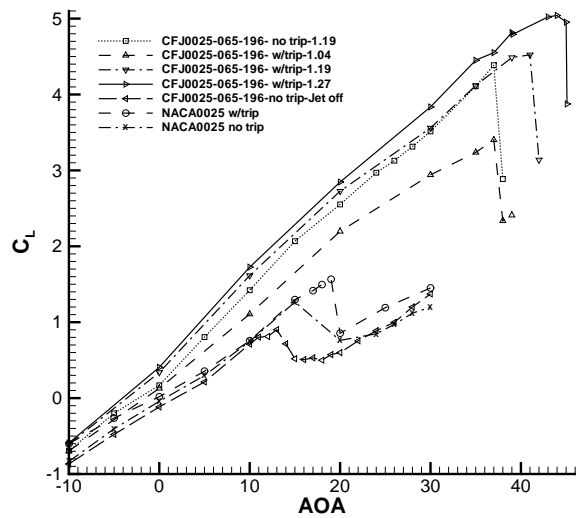


Figure 5: Comparison of the measured lift coefficient for baseline NACA0025 and CFJ0025-065-196 airfoil.

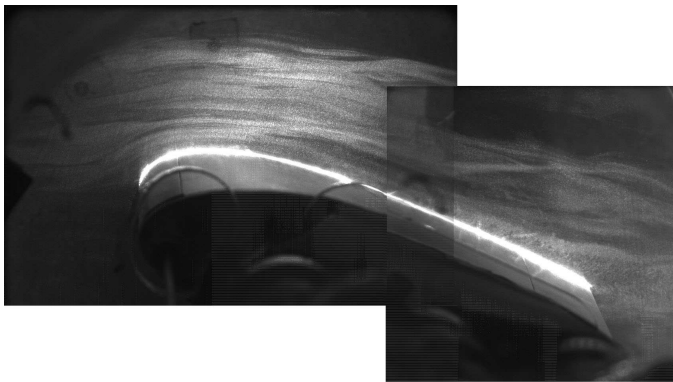


Figure 6: Flow visualization of the attached flow of baseline NACA0025 airfoil at AoA of 10°

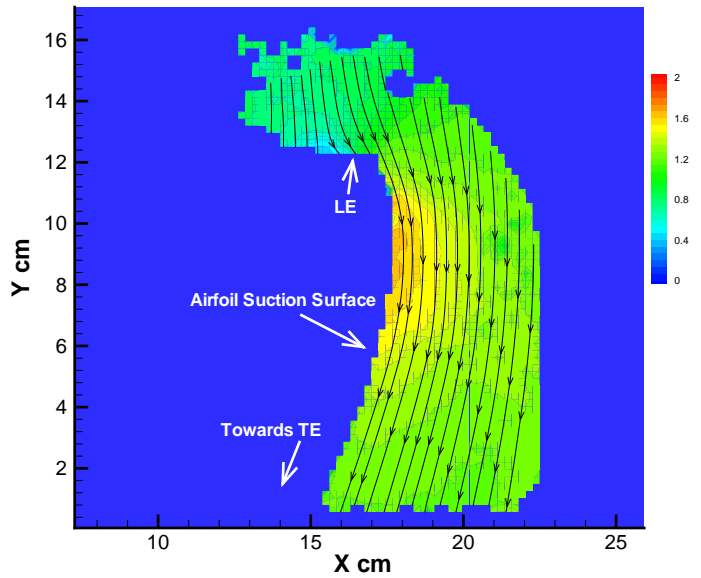


Figure 8: PIV measured normalized velocity (V/V_∞) field of the attached flow of baseline NACA0025 airfoil at AoA of 10° , front portion .

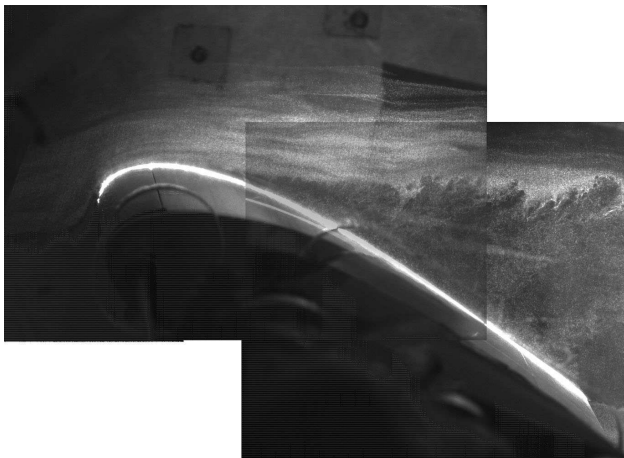


Figure 7: Flow visualization of the separated flow of baseline NACA0025 airfoil at AoA of 10°

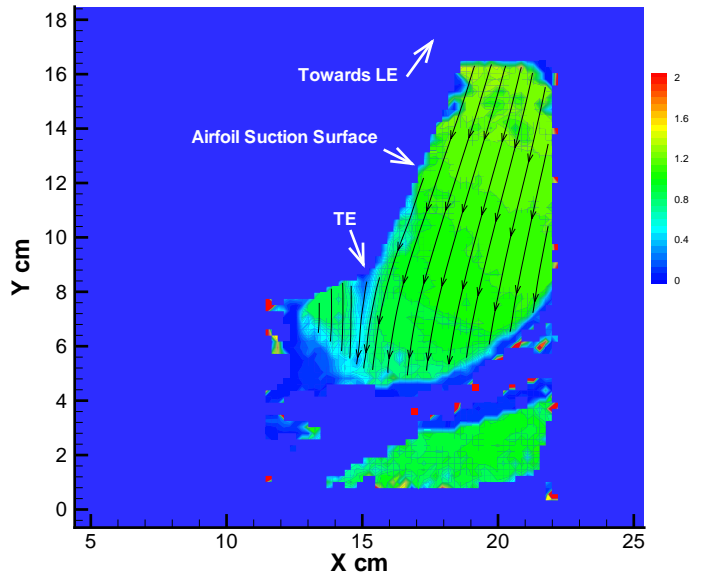


Figure 9: PIV measured normalized velocity (V/V_∞) field of the attached flow of baseline NACA0025 airfoil at AoA of 10° , rear portion .

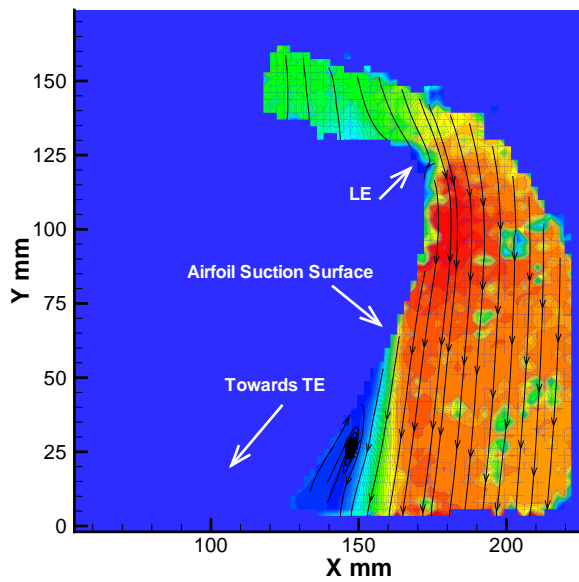


Figure 10: PIV measured normalized velocity (V/V_∞) field of the separated flow of baseline NACA0025 airfoil at AoA of 20°, front portion .

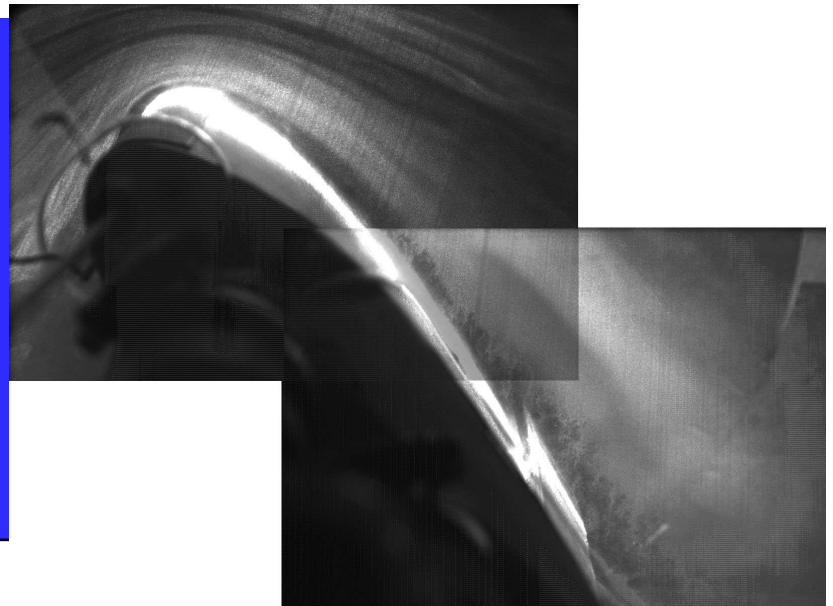


Figure 12: Flow visualization of the attached flow of CFJ0025-065-196 airfoil at AoA of 43°

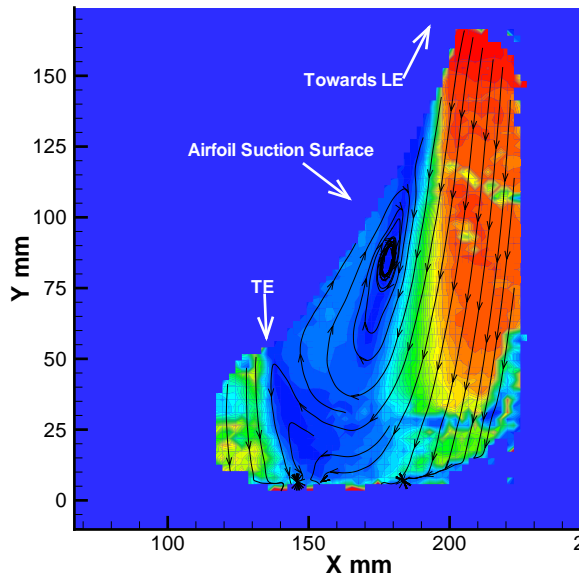


Figure 11: PIV measured normalized velocity (V/V_∞) field of the separated flow of baseline NACA0025 airfoil at AoA of 20°, rear portion .

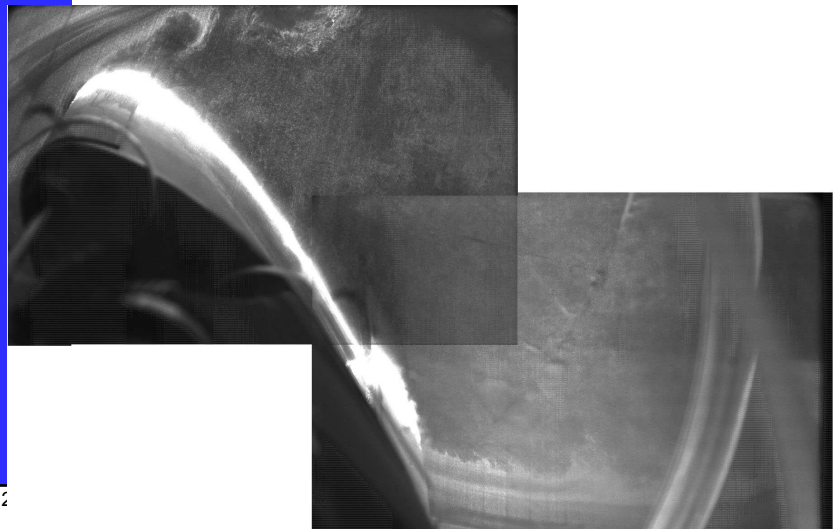


Figure 13: Flow visualization of the separated flow of CFJ0025-065-196 airfoil at AoA of 46° .

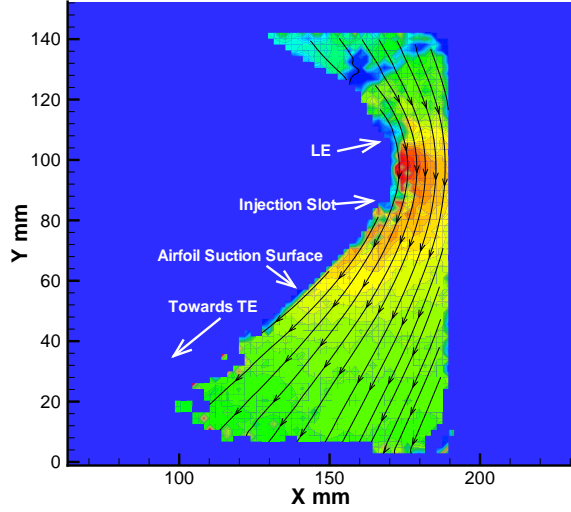


Figure 14: PIV measured normalized velocity (V/V_∞) contours and streamlines of the attached flow of CFJ0025-065-196 airfoil at AoA of 43° , front portion.

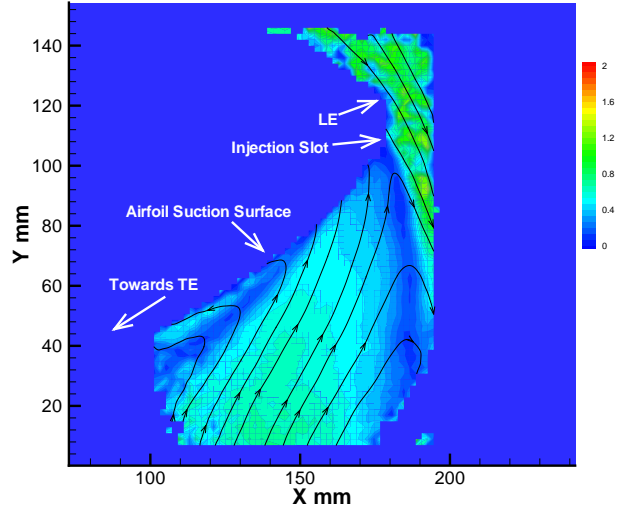


Figure 16: PIV measured normalized velocity (V/V_∞) contours and streamlines of the separated flow of CFJ0025-065-196 airfoil at AoA of 46° , front portion.

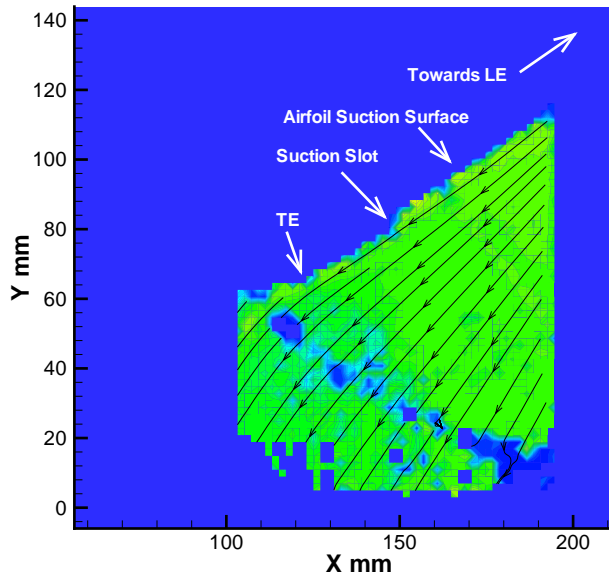


Figure 15: PIV measured normalized velocity (V/V_∞) contours and streamlines of the attached flow of CFJ0025-065-196 airfoil at AoA of 43° , rear portion.

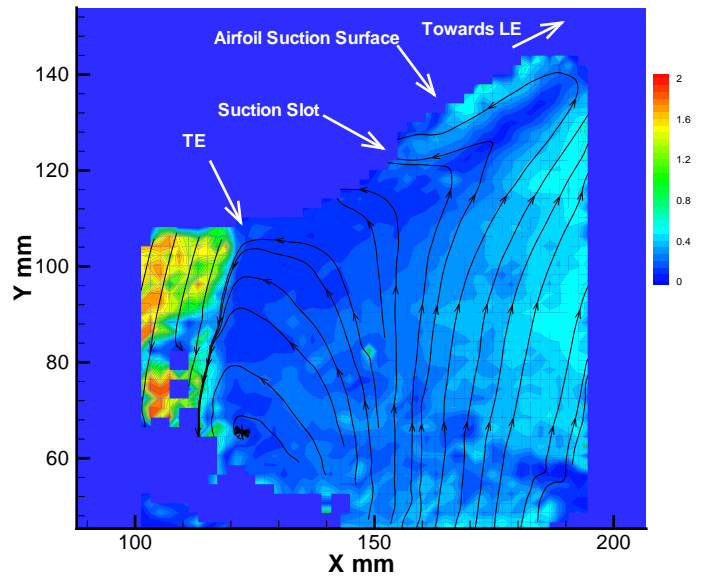


Figure 17: PIV measured normalized velocity (V/V_∞) contours and streamlines of the separated flow of CFJ0025-065-196 airfoil at AoA of 46° , rear portion.

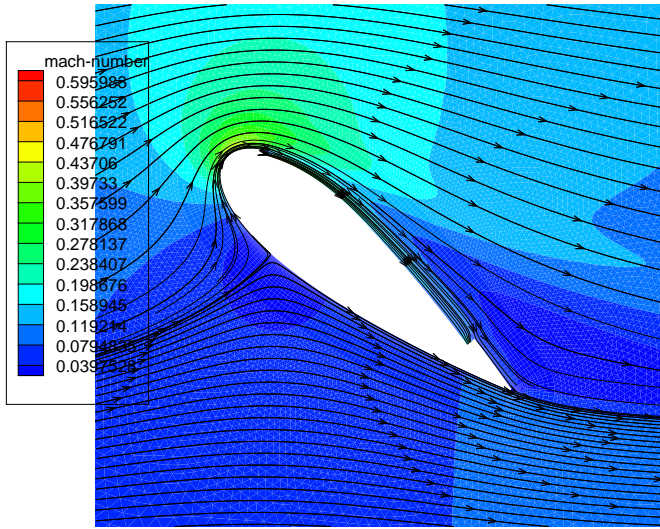


Figure 18: CFD calculated streamlines and Mach contours of the CFJ0025-065-196 airfoil flow field at AoA of 39°.

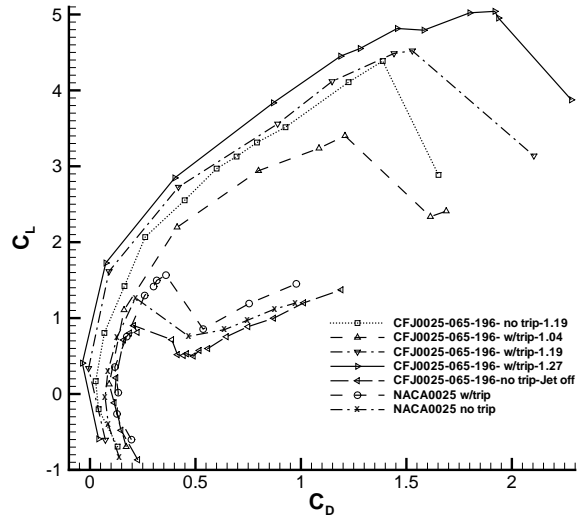


Figure 20: Measured drag polar of CFJ0025-065-196 airfoil.

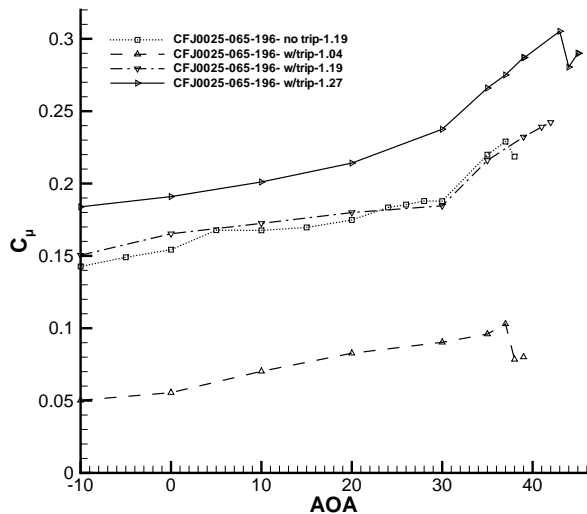


Figure 19: Measured injection momentum coefficient for CFJ0025-065-196 airfoil.

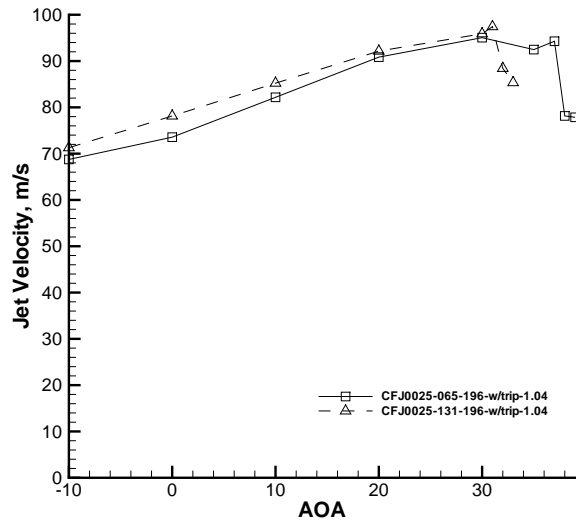


Figure 21: Measured injection jet velocity of CFJ0025-065-196 and CFJ0025-131-196 airfoil with the same injection total pressure.

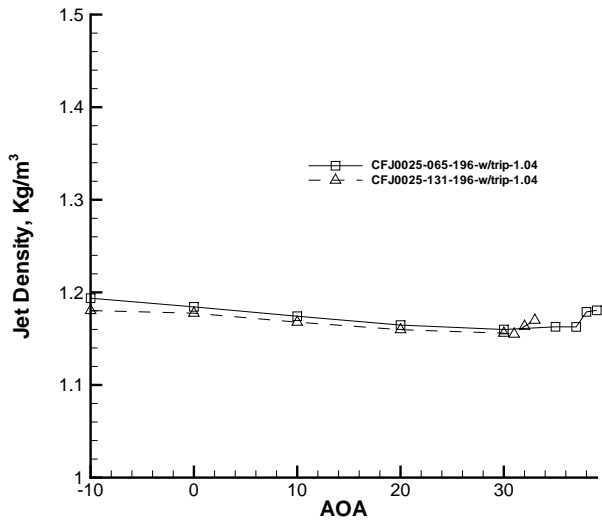


Figure 22: Measured injection jet density of CFJ0025-065-196 and CFJ0025-131-196 airfoil with the same injection total pressure.

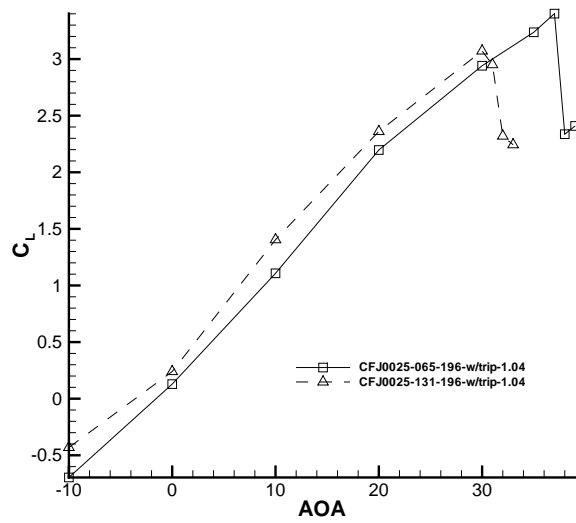


Figure 24: Measured lift coefficient of CFJ0025-065-196 and CFJ0025-131-196 airfoil with the same injection total pressure.

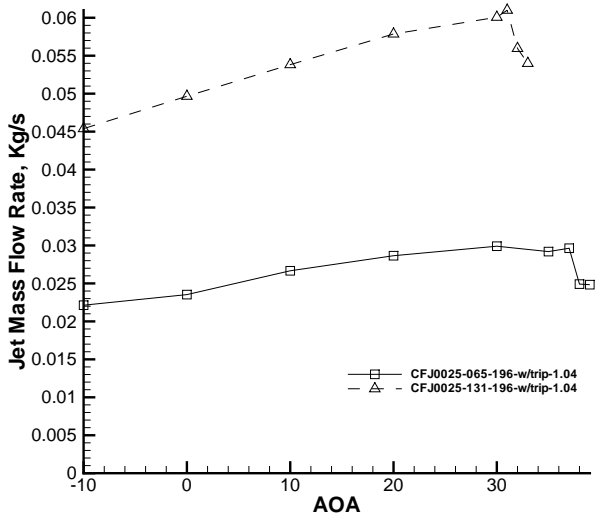


Figure 23: Measured injection mass flow rate of CFJ0025-065-196 and CFJ0025-131-196 airfoil with the same injection total pressure.

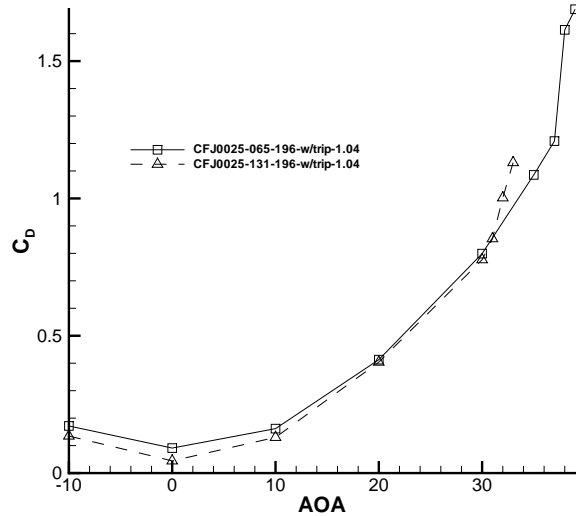


Figure 25: Measured drag coefficient of CFJ0025-065-196 and CFJ0025-131-196 airfoil with the same injection total pressure.

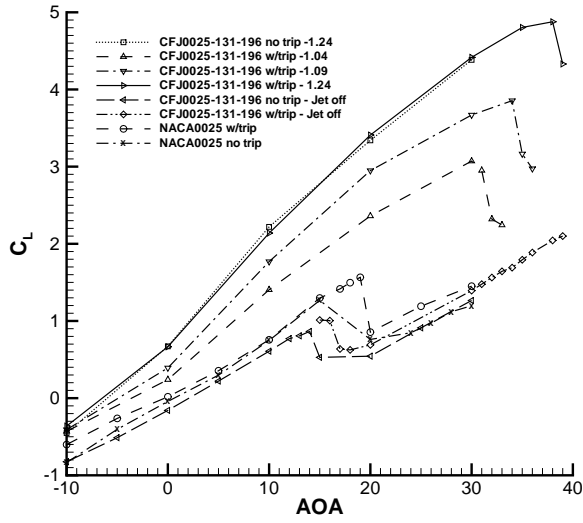


Figure 26: Comparison of the measured lift coefficient for NACA0025 and CFJ0025-131-196 airfoil.

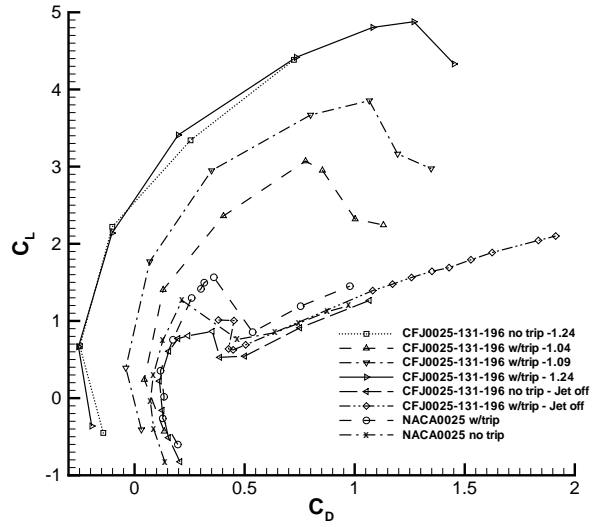


Figure 28: Measured drag polar of CFJ0025-131-196 airfoil.

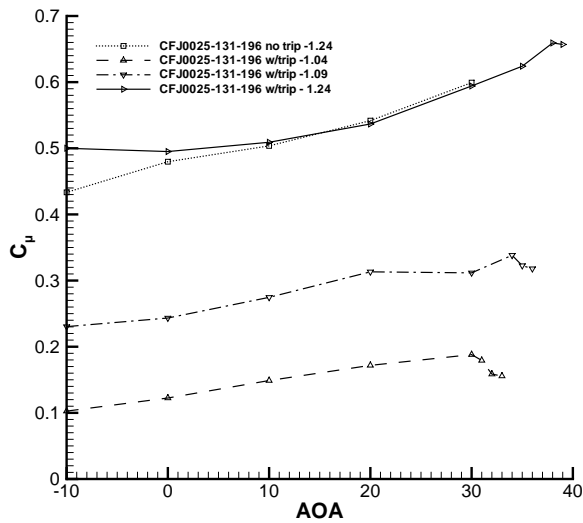


Figure 27: Measured injection momentum coefficient of CFJ0025-131-196 airfoil.

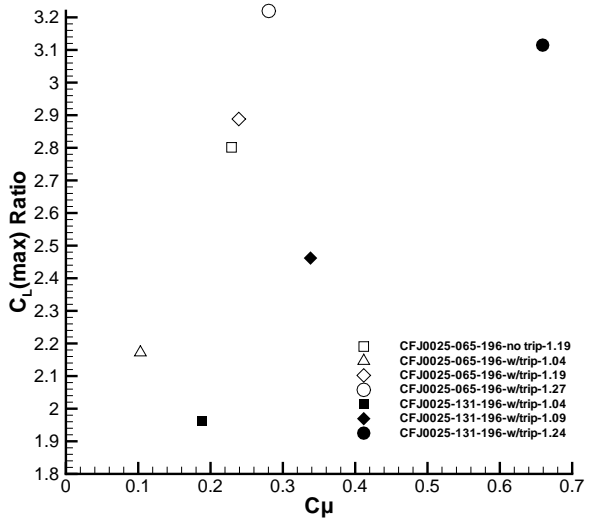


Figure 29: Measured ratio of $C_{Lmaxcfj}/C_{Lmaxbaseline}$ vs jet momentum coefficient for both CFJ0025-096-196 and CFJ0025-131-196 airfoil.

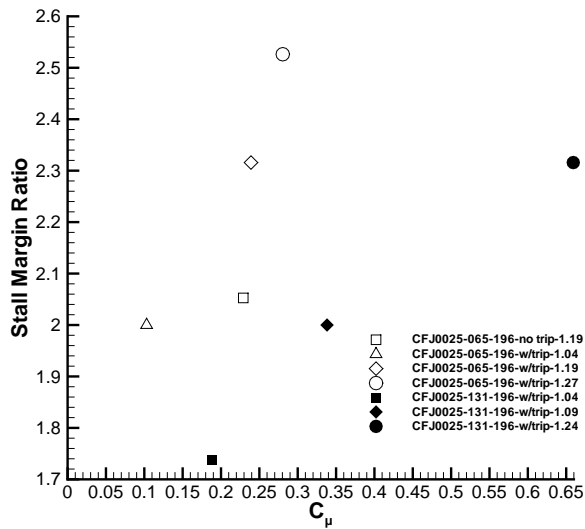


Figure 30: Measured ratio of AoA $stallmargin_{cfj}/stallmargin_{baseline}$ vs jet momentum coefficient for both CFJ0025-096-196 and CFJ0025-131-196 airfoil.

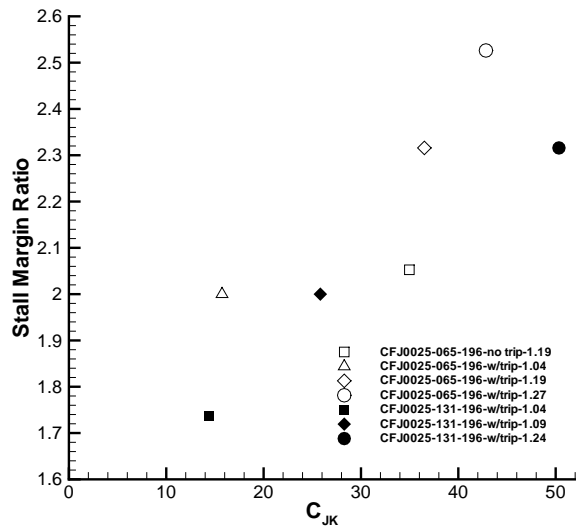


Figure 32: Measured ratio of AoA $stallmargin_{cfj}/stallmargin_{baseline}$ vs jet kinetic energy coefficient for both CFJ0025-096-196 and CFJ0025-131-196 airfoil.

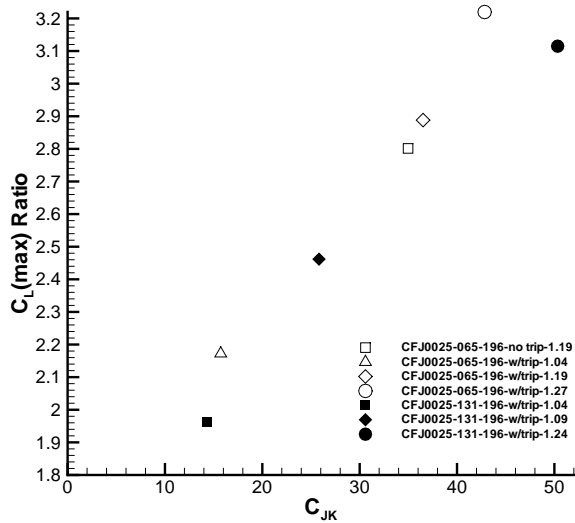


Figure 31: Measured ratio of $C_{Lmaxcfj}/C_{Lmaxbaseline}$ vs jet kinetic energy coefficient for both CFJ0025-096-196 and CFJ0025-131-196 airfoil.

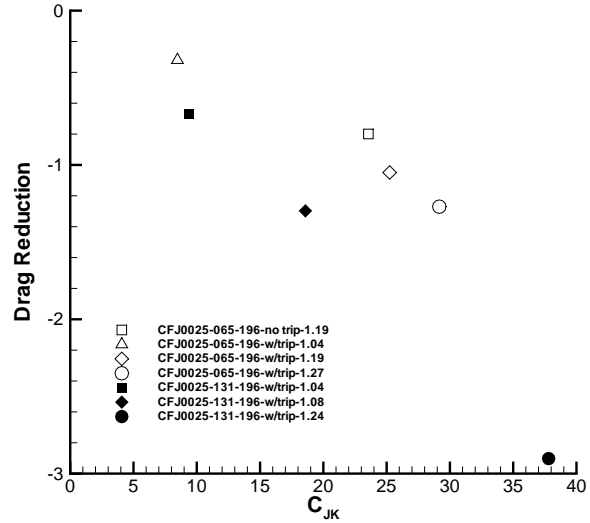


Figure 33: Measured reduction of minimum drag vs jet kinetic energy coefficient at AoA = 0 for both CFJ0025-096-196 and CFJ0025-131-196 airfoil.

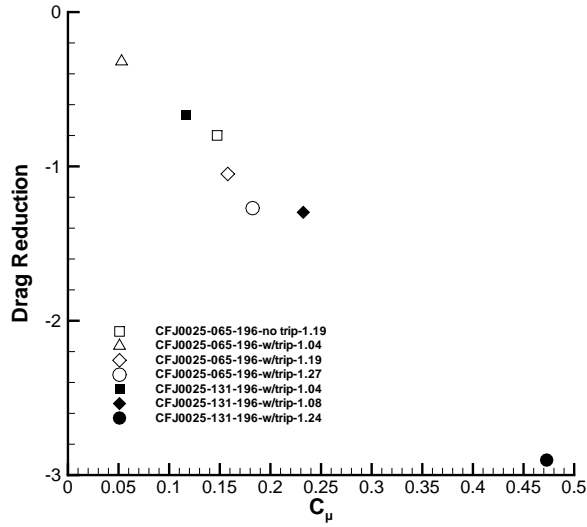


Figure 34: Measured reduction of minimum drag vs momentum coefficient at AoA = 0 for both CFJ0025-096-196 and CFJ0025-131-196 airfoil.

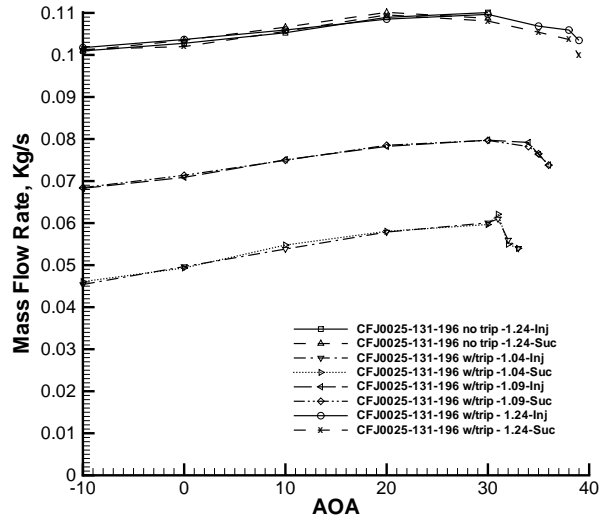


Figure 36: Measured CFJ injection and suction mass flow rate of CFJ0025-131-196 airfoil.

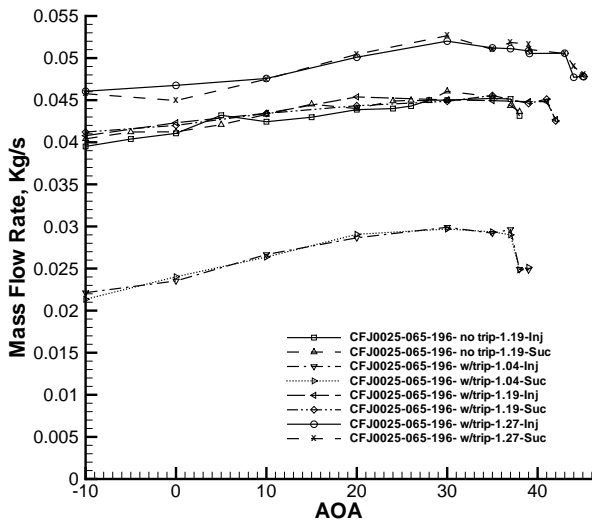


Figure 35: Measured CFJ injection and suction mass flow rate of CFJ0025-096-196 airfoil.

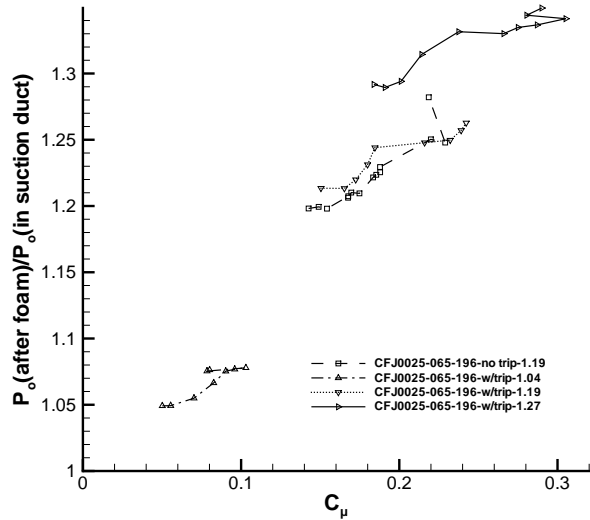


Figure 37: Measured total pressure ratio at CFJ injection and suction for CFJ0025-065-196 airfoil.

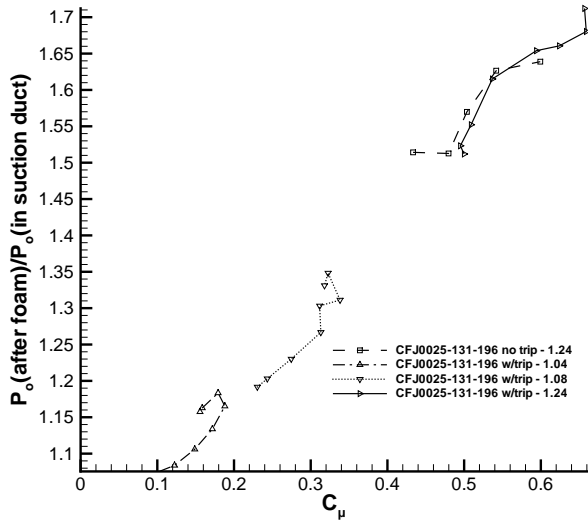


Figure 38: Measured total pressure ratio at CFJ injection and suction for CFJ0025-131-196 air-foil.

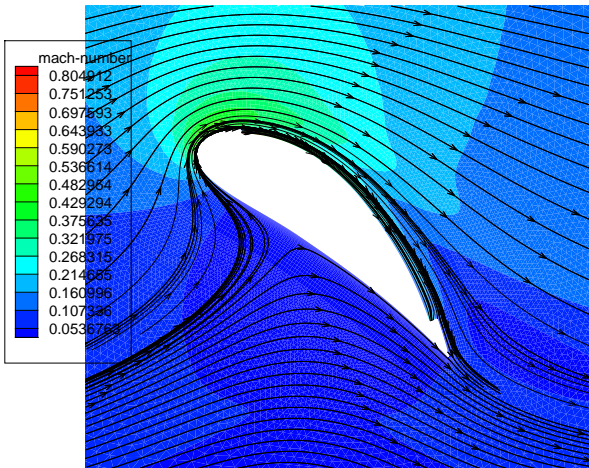


Figure 39: CFD calculated streamlines and Mach contours of the CFJ11425-065-196 airfoil flow field at AoA of 39°.